ELSEVIER

Journal of Electrostatics 56 (2002) 235–254

Journal of
ELECTROSTATICS

www.elsevier.com/locate/elstat

# Numerical solution of the dielectrophoretic and travelling wave forces for interdigitated electrode arrays using the finite element method

N.G. Green[a,b], A. Ramos[a], H. Morgan[b,*]

[a] *Dpto. Electronica y Electromagnetismo, Facultad de Fisica, Universidad de Sevilla, Avenida de Reina Mercedes sln, 41012 Sevilla, Spain*

[b] *Department of Electronics and Electrical Engineering, University of Glasgow, Rankine Building, Oakfield Avenue, Glasgow, Scotland, UK GU2 7KH*

Received 10 July 2001; received in revised form 8 January 2002; accepted 8 January 2002

**Abstract**

AC electrokinetics is the study of the movement of polarisable particles under the influence of AC electric fields. The fields are applied to a suspension of particles by planar microelectrode structures and one particular design, the interdigitated bar electrode has been used in both dielectrophoretic (DEP) field flow fractionation and travelling wave dielectrophoresis. This paper presents, numerical solutions of the DEP and travelling wave forces for an interdigitated electrode array energised with either a 2- or 4-phase signal. The electrorotational torque experienced by the particle in the 4-phase travelling wave array is also calculated. The solutions are compared with previous results. © 2002 Elsevier Science B.V. All rights reserved.

*Keywords:* Dielectrophoresis; Travelling wave fields; Finite element method; Planar electrodes; Particle electrorotational torque; AC electrokinetics

## 1. Introduction

AC electrokinetic forces are produced by the interaction of non-uniform AC electric fields with polarisable particles [1,2], providing a method for controlled movement. Techniques based on these forces have been used for the analysis and

*Corresponding author. Tel.: +44-141-330-5237; fax: +44-141-330-4907.
*E-mail addresses:* n.green@elec.gla.ac.uk (N.G. Green), h.morgan@elec.gla.ac.uk (H. Morgan).

0304-3886/02/$ - see front matter 
PII: S0304-3886(02)00069-4

separation of a range of particle types, particularly biological particles such as cells, bacteria and viruses [2–4]. Dielectrophoretic (DEP) field flow fractionation experiments and travelling wave dielectrophoresis (twDEP) are frequently used in these applications. Both techniques use long arrays of interdigitated bar electrodes fabricated on planar surfaces, in the first case with relative phases of $0^\circ$ and $180^\circ$ applied alternately to the electrodes [5,6] and in the second case, four signals with a successive phase shift of $90^\circ$ are applied to consecutive electrodes [7,8].

Since the forces in AC electrokinetics are generated by the application of an electric field, the strength and direction of the field are required for the analysis of the experimental results. Although the bar electrode array has a simple geometry, neither the electric potential nor the field has an analytical expression. An analytical approximation for the potential and forces in the electrode array has been demonstrated using series expansion, both using Green's functions [9] and Fourier series [10,11]. It should be noted that both of these are approximations to a geometry for which an analytical representation has not been determined.

Numerical methods, such as point charge, charge density, finite difference and integral equation methods have been used to determine electric fields and DEP forces from electrode arrays [12–14].

This paper presents results of the numerical solution of the potential, electric field and the DEP force in the DEP and twDEP electrode arrays using the finite element method [15]. The force equations are re-written to obtain expressions for the force in terms of the real and imaginary components of the field phasor [16,17]. This approach permits the solution of the time-averaged DEP force, as well as the electrorotational torque, in a single step.

For the work presented in this paper, the commercially available Finite Element Solver FlexPDE® (PDE Solutions Inc., USA) [18] was used. This package is a generic partial differential equation (PDE) solver. In two-dimensional problems, the program generates a mesh of triangular elements with second- or third-order polynomial functions. Here third-order polynomials were used.

The solutions are then compared with analytically and numerically calculated values. The validity of the numerical solutions and the importance of the boundary conditions are discussed.

## 2. Theory

### 2.1. Background to the electrical problem

In order to determine the electric field and the electrokinetic forces, the electrical potential is solved for a defined space and set of boundary conditions that represent the electrode array. In this paper phasor notation will be used, with an arbitrary potential oscillating at frequency $\omega$ defined as

$$\phi(\mathbf{x}, t) = \mathrm{Re}[\tilde{\phi}(\mathbf{x})\mathrm{e}^{\mathrm{i}\omega t}], \tag{1}$$

where $i^2 = -1$, $\mathbf{x}$ is the position, Re[...] indicates the real part of and the tilde indicates the phasor $\tilde{\phi} = \phi_R + i\phi_I$. The electric field is then given by $\mathbf{E}(\mathbf{x}, t) = \mathrm{Re}[\tilde{\mathbf{E}}(\mathbf{x})e^{i\omega t}]$ where the vector $\tilde{\mathbf{E}} = -\nabla\tilde{\phi} = -(\nabla\phi_R + i\nabla\phi_I)$ is the corresponding phasor.

For currents and frequencies typically found in AC electrokinetic problems, Maxwell's equations can be reduced to the quasi-electrostatic form [17].

$$\mathbf{E} = -\nabla\phi, \qquad \text{the electric field is irrotational,}$$

$$\nabla \cdot \mathbf{J} + \frac{\partial \rho}{\partial t} = 0, \qquad \text{the charge conservation equation,}$$

$$\nabla \cdot \mathbf{D} = \rho, \qquad \text{Gauss's equation,}$$

where $\mathbf{J}$ is the conduction current, $\rho$ is the free charge density and $\mathbf{D}$ is the electric flux density or the displacement vector. For a homogeneous linear dielectric with permittivity $\varepsilon$ and conductivity $\sigma$, $\mathbf{J} = \sigma\mathbf{E}$ and $\mathbf{D} = \varepsilon\mathbf{E}$, and the equation for the potential phasor is

$$\nabla \cdot ((\sigma + i\omega\varepsilon)\nabla\tilde{\phi}) = 0. \tag{2}$$

For a homogeneous medium, this reduces to Laplace's equation for the real and imaginary components of the phasor, respectively

$$\nabla^2\phi_R = 0 \quad \text{and} \quad \nabla^2\phi_I = 0. \tag{3}$$

In this work these equations, together with boundary conditions appropriate to the particular type of electrodes array, are solved by the finite element solver.

### 2.2. The dielectrophoretic force

The DEP force arises from the interaction of the non-uniform electric field and the dipole moment induced in the particle, assuming that the higher order terms can be neglected [1,2]. For linear, isotropic dielectrics and an applied potential of a single frequency, the relationship between the electric field phasor $\tilde{\mathbf{E}}$ and the dipole moment phasor $\tilde{\mathbf{p}}(\omega)$ for a spherical particle is $\tilde{\mathbf{p}}(\omega) = \upsilon\alpha(\omega)\tilde{\mathbf{E}}$, where $\alpha$ is the effective polarisability of the particle and $\upsilon$ is the volume of the particle. The time-averaged force on the particle is given by [1]

$$\langle \mathbf{F} \rangle = \tfrac{1}{2}\,\mathrm{Re}[(\tilde{\mathbf{p}} \cdot \nabla)\tilde{\mathbf{E}}^*]. \tag{4}$$

Substituting for the dipole moment phasor $\tilde{\mathbf{p}}$, this expression can be re-written and simplified to the expression $2\upsilon\alpha(\tilde{\mathbf{E}} \cdot \nabla)\tilde{\mathbf{E}}^* = \upsilon\alpha\nabla(\tilde{\mathbf{E}} \cdot \tilde{\mathbf{E}}^*) - \upsilon\alpha\nabla \times (\tilde{\mathbf{E}} \times \tilde{\mathbf{E}}^*)$. Here, two vector identities have been used: first $\nabla(\mathbf{A} \cdot \mathbf{B}) = (\mathbf{B} \cdot \nabla)\mathbf{A} + (\mathbf{A} \cdot \nabla)\mathbf{B} + \mathbf{B} \times (\nabla \times \mathbf{A}) + \mathbf{A} \times (\nabla \times \mathbf{B})$ with the fact that the electric field is irrotational, i.e. $\nabla \times \tilde{\mathbf{E}} = 0$; second $\nabla \times (\mathbf{A} \times \mathbf{B}) = (\mathbf{B} \cdot \nabla)\mathbf{A} - (\mathbf{A} \cdot \nabla)\mathbf{B} + (\nabla \cdot \mathbf{B})\mathbf{A} - (\nabla \cdot \mathbf{A})\mathbf{B}$ with Gauss's law with zero free charge density, i.e. $\nabla \cdot \tilde{\mathbf{E}} = 0$. The time-averaged force is then [19]

$$\langle \mathbf{F} \rangle = \tfrac{1}{4}\upsilon\,\mathrm{Re}[\alpha\nabla(\tilde{\mathbf{E}} \cdot \tilde{\mathbf{E}}^*)] - \tfrac{1}{2}\upsilon\,\mathrm{Re}[\alpha\nabla \times (\tilde{\mathbf{E}} \times \tilde{\mathbf{E}}^*)]. \tag{5}$$

The first term on the right-hand side is the DEP force experienced in an electric field with a spatially varying magnitude but with no spatial variation in phase, such as

that used in DEP field flow fractionation. In this case, the second component is zero. In an electric field with a spatial phase variation such as in twDEP, the second term is non-zero. This expression is equivalent to what Wang et al. refer to as general dielectrophoresis [20].

In this paper, the two components of the force will be considered separately for ease of reference and will be referred to as the DEP and twDEP components of the force. Inserting the expressions for the phasors gives:

$$\begin{aligned}\langle \mathbf{F}_{\mathrm{DEP}} \rangle &= \tfrac{1}{4}\upsilon \,\mathrm{Re}[\alpha]\nabla(|\mathrm{Re}[\tilde{\mathbf{E}}]|^2 + |\mathrm{Im}[\tilde{\mathbf{E}}]|^2) \\ &= \tfrac{1}{4}\upsilon \,\mathrm{Re}[\alpha]\nabla(|\nabla\phi_{\mathrm{R}}|^2 + |\nabla\phi_{\mathrm{I}}|^2),\end{aligned} \tag{6}$$

$$\begin{aligned}\langle \mathbf{F}_{\mathrm{twDEP}} \rangle &= -\tfrac{1}{2}\upsilon \,\mathrm{Im}[\alpha](\nabla \times (\mathrm{Re}[\tilde{\mathbf{E}}] \times \mathrm{Im}[\tilde{\mathbf{E}}])) \\ &= -\tfrac{1}{2}\upsilon \,\mathrm{Im}[\alpha](\nabla \times (\nabla\phi_{\mathrm{R}} \times \nabla\phi_{\mathrm{I}})).\end{aligned} \tag{7}$$

The expressions $\mathrm{Re}[\tilde{\mathbf{E}}] = -\nabla\phi_{\mathrm{R}}$ and $\mathrm{Im}[\tilde{\mathbf{E}}] = -\nabla\phi_{\mathrm{I}}$ refer to the real and imaginary components of the electric field phasor, respectively.

The electrorotational torque [1] can also be calculated for the case of the travelling wave array, or indeed for any system with a spatially varying phase. The torque is given by

$$\begin{aligned}\langle \boldsymbol{\Gamma} \rangle &= \tfrac{1}{2}\mathrm{Re}[\tilde{\mathbf{p}} \times \tilde{\mathbf{E}}^*] = \tfrac{1}{2}\upsilon \,\mathrm{Re}[\alpha\tilde{\mathbf{E}} \times \tilde{\mathbf{E}}^*] \\ &= \upsilon \,\mathrm{Im}[\alpha](\nabla\phi_{\mathrm{R}} \times \nabla\phi_{\mathrm{I}}).\end{aligned} \tag{8}$$

It should be noted that measurement of the rate of rotation during a twDEP experiment would give an independent means of determining $\mathrm{Im}[\alpha]$ for the particle.

The expressions given for the force and torque here (Eqs. (6)–(8)) are suitable for the numerical method used in this work. Since the boundary conditions for the real and imaginary parts of the complex phasor can be independently and completely defined, the real and imaginary parts of the phasor can be solved independently. The resulting solutions for the phasor can then be used to determine the time-averaged forces and torque without involving a time stepped calculation such as used in Ref. [14].

### 2.3. Boundary conditions and simplifications

#### 2.3.1. General

There are several boundary conditions common to both the two-electrode dielectrophoresis array and the four-electrode travelling wave array, which are therefore specified the same way for both problems.

First, since the electrodes are long compared to their width, the problem can be considered to be two dimensional.

At heights much greater than the typical electrode dimension, the potential and the electric field both go to zero. In the numerical problem, if the upper boundary is sufficiently far from the electrodes, either a Dirichlet condition ($\tilde{\phi} = 0$) or a Neumann condition $\partial\tilde{\phi}/\partial n = 0$ can be specified.

The electrodes are considered to be infinitely thin, a valid approximation since the thickness of the electrode is $\sim 100\,\text{nm}$ and the width of the gaps/electrodes greater than $\sim 10\,\mu\text{m}$. The electrodes are therefore represented by a section of the bottom boundary with an appropriate value of the potential. It is important to note that the resulting solution will be incorrect very close to the electrode edges, as discussed in [9] since the numerical problem is different from the experimental situation. However, in this region the rapid variation of the electric field means that the dipole approximation for the DEP force is invalid, and so inaccuracies in the field solution are not so important.

The remainder of the lower boundary represents the interface between the electrolyte above the electrodes and the glass of the substrate below. The condition at this interface is that both the potential and the normal component of the total current (conduction plus displacement) are continuous. This can be simplified to a Neumann boundary condition for the potential in the electrolyte ($\partial\tilde{\phi}/\partial n = 0$, where $\hat{\mathbf{n}}$ is the normal to the boundary) by the following argument. The normal component of the total current must be continuous, i.e.

$$(\sigma_g + i\omega\varepsilon_g)\tilde{\mathbf{E}}_g \cdot \hat{\mathbf{n}} = (\sigma_{el} + i\omega\varepsilon_{el})\tilde{\mathbf{E}}_{el} \cdot \hat{\mathbf{n}}, \tag{9}$$

where the subscript g signifies glass and el electrolyte. Values of the conductivity of an electrolyte are $\sigma_{el} = 10^{-4}-10^{-1}\,\text{Sm}^{-1}$ and the conductivity of glass can be considered to be zero. The relative permittivity of water is $\sim 80$ and of glass is $\sim 3$. Putting these values in Eq. (9) it can be seen that the normal component of the electric field in the electrolyte at the interface is negligible compared to that of the glass for all frequencies. Therefore, the solution space can be simplified to just the electrolyte with the condition $\partial\tilde{\phi}/\partial n = 0$ on the lower boundary between the electrodes. This is also the exact boundary condition if two semi-infinite media are considered (water and glass separated by a flat interface). In this case, the potential can be considered to be created by a 2D charge distribution on the electrodes and these charges will always generate a field tangential to the plane of the electrodes. This is not true for finite media since image charges are induced on the top and bottom interfaces.

In Ref. [11], the lower boundary condition was assumed to be a linear change in potential between the electrodes. In this paper, the potential, fields and forces will also be solved with this boundary condition and compared with the Fourier series analysis of Ref. [11]. This comparison is necessary in order to validate the numerical calculation of the forces and also to estimate the error of the numerical solution.

The remaining boundary conditions, i.e. those for the sides of the problem and for the potential on the different electrodes, depend on the configuration of the electrodes and the applied signals.

### 2.3.2. The dielectrophoretic array

The values for the real and imaginary parts of the potential phasor at the electrodes are shown in Fig. 1a. Since for this array there are only two signals with a difference in phase of 180°, the problem has a spatially independent phase. As can be seen, $\phi_I$ is zero and only $\phi_R$ needs to be solved, with the boundary conditions as shown in the figure.

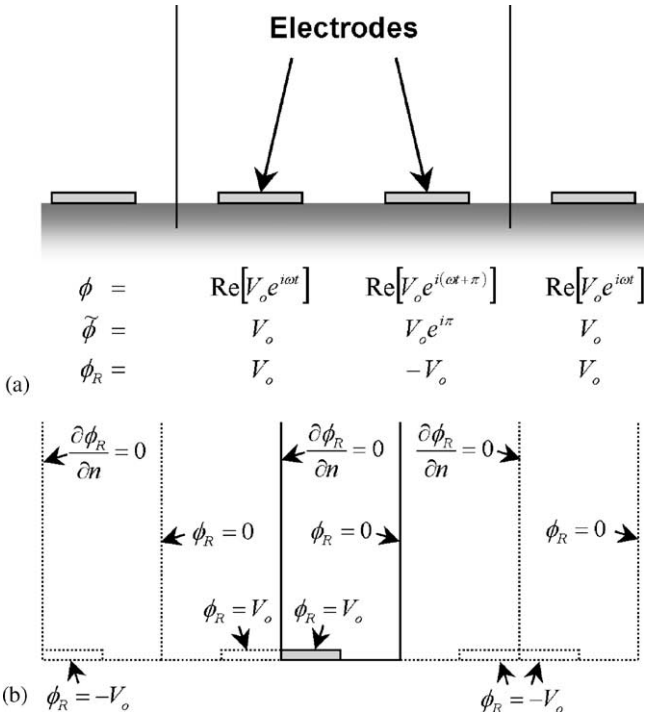


Fig. 1. (a) A schematic diagram of the electrode array with 2-phases applied as in dielectrophoresis experiments. The vertical lines mark the period over which the system repeats. Also shown are the values for the potential $\phi$, the potential phasor $\tilde{\phi}$ and the value of $\phi_R$ on each electrode. The imaginary part of the phasor, $\phi_I$, is zero everywhere. (b) The smallest possible problem space required for correct solution of the problem. The solid lines indicate this unit cell with a line of even symmetry on the left and even symmetry on the right and the single half-electrode required. The dotted lines indicate the images of the unit cell demonstrating that the problem is completely described.

The boundary conditions repeat every second electrode and are symmetrical, implying that the problem space does not need to be larger than two electrodes. The problem space can be further reduced to a quarter of this size using symmetry planes as shown in Fig. 1b. The basic cell covers one half of one electrode, chosen arbitrarily in this case to be that with positive potential $V_0$, and half of the adjacent gap. The vertical edge of the problem space running through the electrode is a line of even symmetry, i.e. $\partial\phi_R/\partial n = 0$ and that running through the centre of the gap is a line of odd symmetry, $\phi_R = 0$.

### *2.3.3. The travelling wave array*

The values for the real and imaginary parts of the potential phasor at the electrodes are as shown in Fig. 2a. The basic problem space covers four adjacent electrodes, after which the boundary conditions on the electrodes repeat. Further simplifications can be made to the problem space using other symmetries. The

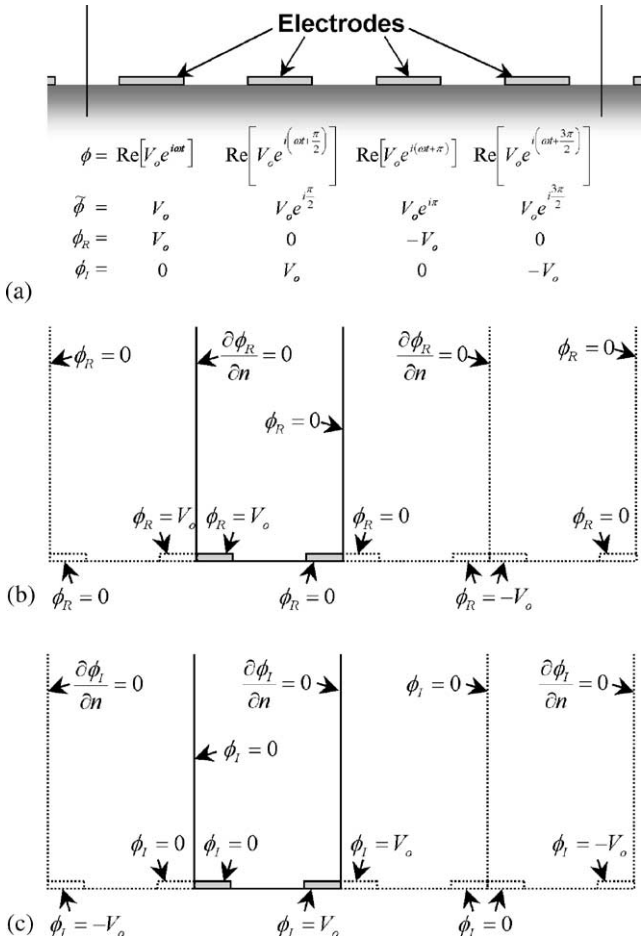


Fig. 2. (a) A schematic diagram of the 4-phase travelling wave electrode array where the vertical lines indicate the length over which the system repeats. Also shown are the values for the potential $\phi$, the potential phasor $\tilde{\phi}$ and the real, $\phi_R$, and imaginary, $\phi_I$, parts the potential phasor. The basic unit cell for the travelling wave electrode array (indicated by the solid lines) with the boundary conditions for the real part of the potential phasor is shown in (b) and for the imaginary part in (c). The dotted lines demonstrate how the mirror planes describe the complete electrode array.

minimum problem space that must be solved is one quarter of the four-electrode space as shown in Fig. 2b and c, covering the region between the centres of *two* adjacent electrodes and the entire gap between. In this paper, the electrodes in the solution space were chosen to be $0^\circ$ and $90^\circ$. The rest of the problem space is defined using even and odd symmetry boundary conditions. Fig. 2b shows the basic cell for the real part of the phasor $\phi_R$ with the boundary conditions and the "images" of the potentials created by the symmetry boundaries. Fig. 2c shows the same scheme for the imaginary part of the phasor $\phi_I$. This defines the complete problem in this case.

Comparison of Fig. 2b and c shows that the conditions for $\phi_I$ are the mirror image of those for $\phi_R$ about the centre of the gap. This implies that the solution for $\phi_I$ will also be the mirror image of $\phi_R$ about the same line. Therefore, only $\phi_R$ needs to be solved, the solution then being mirrored around the vertical line through the middle of the gap to give $\phi_I$.

### 2.4. Non-dimensional equations

A method for avoiding extreme numbers in numerical calculations is to scale the variables according to typical values. In this paper, the potential will be scaled with $V_0$, the amplitude of the applied signals, and the distances will be scaled with $d$, the distance between the centre of the electrode and the centre of the adjacent gap. This gives the non-dimensional potential $\tilde{\phi}' = \tilde{\phi}/V_0$ and displacement $\mathbf{x}' = \mathbf{x}/d$. The non-dimensional potentials also satisfy Laplace's equation

$$\frac{V_0}{d^2}\nabla'^2\tilde{\phi}' = 0 \Rightarrow \nabla'^2\tilde{\phi}' = 0.$$

The expressions for the force components are then

$$\langle \mathbf{F}_{DEP} \rangle = \tfrac{1}{4}\upsilon \,\mathrm{Re}[\alpha]\frac{V_0^2}{d^3}\nabla'(|\nabla'\phi'_R|^2 + |\nabla'\phi'_I|^2), \tag{10}$$

$$\langle \mathbf{F}_{twDEP} \rangle = -\tfrac{1}{2}\upsilon \,\mathrm{Im}[\alpha]\frac{V_0^2}{d^3}(\nabla' \times (\nabla'\phi'_R \times \nabla'\phi'_I)).$$

The potential only has to be solved once for any particular ratio of electrode/gap width. The resulting non-dimensional solution can then be scaled for any distance $d$, applied potential $V_0$, particle volume $\upsilon$ or effective frequency-dependent polarisability $\alpha$.

## 3. The dielectrophoretic array—results and discussion

Fig. 3 shows the problem space for the DEP array with the complete boundary conditions for the potential $\phi'_R$: on the electrode $\phi'_R = 1$; on the left hand and upper edges $\partial\phi'_R/\partial n = 0$; and at the right-hand edge $\phi'_R = 0$. The condition on the bottom edge between the electrodes was $\partial\phi'_R/\partial n = 0$. The distance along the base of the solution space is $d$, which is 1 in dimensionless units, the electrode width is $d_1$ and the gap width is $d_2$. Initially, the problem was solved with $d_1 = d_2 = d$. The height $h$ of the solution space is required to be much greater than $d$ and was set to be 10.

### 3.1. Results

The potential and magnitude of the electric field are shown in Fig. 4a and b. The vector $\nabla'|\nabla'\phi'_R|^2$ in the expression for the DEP force is shown in Fig. 4c, with the direction vectors plotted separately from the magnitude, which is plotted logarithmically as contours. Away from the electrodes, above $y' \sim 1$, the vectors

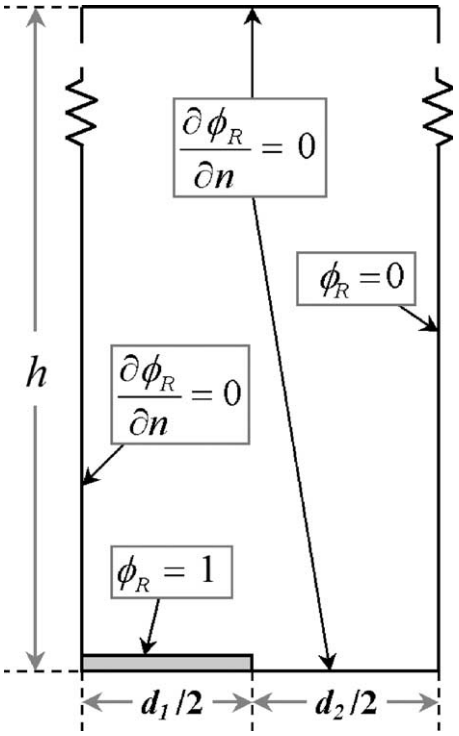


Fig. 3. The problem space for the dielectrophoresis array showing the complete boundary conditions. The space covers one half of an electrode and half of the adjacent gap. The distance along the base is dimensionless length 1, equivalent to characteristic distance $d$. The height $h$ is much greater than the width of the problem space.

point straight towards the electrode plane. Moving downwards from this height, the vectors point more and more towards the electrode edge at $x' = 0.5$. The pattern of the DEP force vectors is symmetrical about a vertical line through the electrode edge, an observation consistent with the fact that the electric field (Fig. 4b) is also symmetrical about the same line. This is different from previous calculations [11] where approximations to the boundary condition between the electrodes were made.

Examining Fig. 4c, it can be seen that above $y' \sim 1$ the magnitude of the vector function is constant with $x$ across the array, as is the magnitude of the electric field. In addition, the magnitudes of the field and $\nabla'|\nabla'\phi'_{\mathrm{R}}|^2$can be matched to an exponentially decreasing function of the height, i.e. of the form

$$f = A\mathrm{e}^{-ky}. \tag{11}$$

According to a general Fourier analysis of the problem, the exponential factor $k$ should be equal to $2\pi/\lambda$, where $\lambda$ is the spatial period of the problem [11]. The magnitudes of the electric field, $\nabla'\phi'_{\mathrm{R}}$ and the vector $\nabla'|\nabla'\phi'_{\mathrm{R}}|^2$ along a vertical line are plotted logarithmically in Fig. 5a and b. As can be seen, above approximately

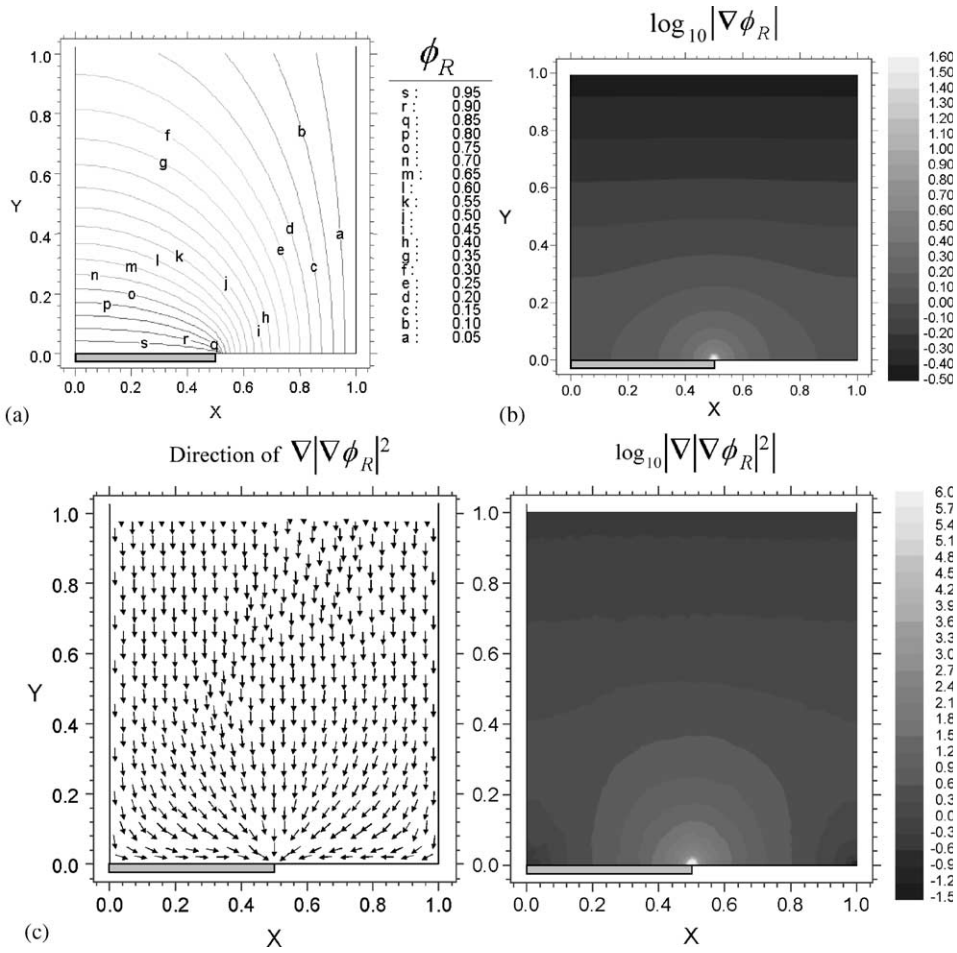


Fig. 4. The solution of the problem in the $1 \times 1$ region close to the electrode. (a) The calculated potential $\phi'_R$ and (b) the electric field magnitude $|\nabla'\phi'_R|$. (c) The vector $\nabla'|\nabla'\phi'_R|^2$ calculated from the potential shown as separate vector direction and magnitude plots. The scale on the magnitude plots for both the field and $\nabla'|\nabla'\phi'_R|^2$ are $\log_{10}$.

$y' = 1$ ($y = d$), the magnitudes can be matched to the exponentially decreasing functions shown in the figures. For the electric field magnitude, the exponential factor $k_E$ was $\pi/2$ and the coefficient $A_E$ was 1.6947. The values of the coefficient and factor for $|\nabla'|\nabla'\phi'_R|^2|$ are shown in Fig. 5b. Re-writing Eq. (6) and substituting for the dimensionless height in the exponential gives the complete expression for the DEP force component in this region:

$$\langle \mathbf{F}_{DEP} \rangle = -A_{DEP}\upsilon \,\mathrm{Re}[\alpha]\frac{V_0^2}{d^3} e^{(-k_{DEP}y/d)}\hat{\mathbf{y}}, \tag{12}$$

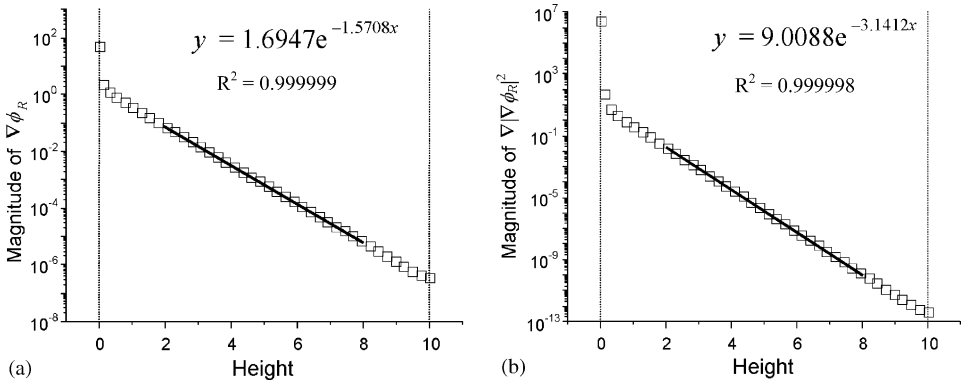


Fig. 5. The magnitude of (a) the electric field $\nabla'\phi'_{\mathrm{R}}$ and (b) $\nabla'|\nabla'\phi'_{\mathrm{R}}|^2$ plotted along a vertical line running through $x' = 0.5$. The scale was $\log_{10}$ and the two magnitudes follow exponentially decreasing functions above $y' \sim 1$.

where $k_{\mathrm{DEP}} = \pi$ and $A_{\mathrm{DEP}} = 2.2534$. These coefficients were calculated from the dimensionless problem and Eq. (12) gives the value of the force for *any* applied potential $V_0$ or $d$ as long as the electrode width to gap width ratio is 1:1.

### 3.2. Comparison with Fourier series solution

Comparison with the values for these constant derived using Fourier series analysis [11] shows a discrepancy. Calculating the value of $A_{\mathrm{E}}$ and $A_{\mathrm{DEP}}$ from the first-order term in the Fourier series gives values of 1.8006 and 2.54648, respectively. Calculating the percentage difference of these values from the numerically calculated values gives 6.3% for $A_{\mathrm{E}}$ and 13.0% for $A_{\mathrm{DEP}}$. This information is summarised in Table 1.

The difference in the values for the coefficient $A_{\mathrm{DEP}}$ arises from the fact that in the Fourier series analysis, the potential was calculated for a different boundary condition between the electrodes. Instead of the Neumann condition used here, the potential was assumed to change linearly along the bottom surface between the electrodes.

In order to validate the numerical method used in this work, the problem was solved a second time using identical boundary conditions to those used for the Fourier series analysis. Again, above $y' = 1$, the magnitude of $\nabla'\phi'_{\mathrm{R}}$ and $\nabla'|\nabla'\phi'_{\mathrm{R}}|^2$ can be matched to Eq. (11). The values of $k_{\mathrm{E}}$ and $k_{\mathrm{DEP}}$ were found to be the same as for the Neumann boundary condition. The numerically determined values of $A_{\mathrm{E}}$ and $A_{\mathrm{DEP}}$ (see Table 1) agree closely with the Fourier series analysis (errors of 0.016% and 0.013%, respectively).

The good agreement with the analytical Fourier series solution demonstrates that the numerical method used here produces valid results with an estimated error of 0.01%. It also shows that the value of the force calculated at distances far from the

Table 1
Numerically calculated values of the coefficients for the exponential approximation of the electric field and the dielectrophoretic force at sufficient distance from the electrodes

| Boundary condition in gap | $k_E$ | $A_E$ | $k_{DEP}$ | $A_{DEP}$ | % difference from Fourier |
|---|---|---|---|---|---|
| Numerical solution: constant current $\partial\phi'_R/\partial n = 0$ | 1.5708 | 1.6947 | 3.1412 | 2.2534 | 13.0 |
| Numerical solution: linear potential | 1.5708 | 1.8009 | 3.1414 | 2.5468 | 0.013 |
| First-order Fourier expansion | $\pi/2$ | 1.8006 | $\pi$ | 2.54648 | |

Table 2
Numerically calculated values of the coefficient $A_{DEP}$ in the exponential approximation of the dielectrophoretic force for a variety of electrode/gap ratios, as well as the values calculated from the Fourier series analysis and the percentage difference

| Electrode/gap ratio $d_1$:$d_2$ | $A_{DEP}$ (numerically determined) | $A_{DEP}$ (Fourier series solution) | % Fourier from numerical |
|---|---|---|---|
| 4:1 | 2.9954 | 3.039588939 | 1.47 |
| 3:1 | 2.9112 | 2.983385829 | 2.48 |
| 2:1 | 2.7339 | 2.864788976 | 4.79 |
| 1:1 | 2.2534 | 2.546479089 | 13.0 |
| 1:2 | 1.6657 | 2.148591732 | 28.0 |
| 1:3 | 1.3448 | 1.932049654 | 43.7 |
| 1:4 | 1.1462 | 1.79946248 | 56.0 |

electrodes is dependent on the boundary condition assigned at $y' = 0$ between the electrodes.

### 3.3. Different electrode/gap width ratios

As a further investigation of the relationship between the DEP force far from the electrodes and the geometry of the electrodes, the problem was solved for different ratios of electrode width $d_1$ to gap width $d_2$. The values for the exponential coefficients $k_{DEP}$ were, for all cases, within 0.03% of $\pi$ as expected. The values of $A_{DEP}$ for several different ratios are shown in Table 2, along with the value calculated from the Fourier series solution together with the difference between the two expressed as a percentage.

As the ratio between the electrode and gap width increases, the numerically calculated value for $A_{DEP}$ increases and the difference between it and the Fourier series value decreases to $\sim$1.5% in the case of a ratio of 4:1. For low values of the ratio, the difference becomes much larger, with a difference of 56% for a ratio of 1:4.

This dependency indicates that as the gap width decreases, the exact boundary condition on the surface between the electrodes becomes less important in determining the force far from the electrodes.

From the experimental point of view, large values of the electrode/gap width ratio might be the best approach since the Fourier series solution can be used to determine particle motion. In addition, the magnitude of the DEP force far from the electrodes is greater.

## 4. The travelling wave array

Although the basic geometry of the twDEP array is the same as the DEP array, a long series of coplanar bar electrodes, the problem space is more complicated.

The minimum problem space for the travelling wave array is shown in Fig. 6 with the boundary conditions for the potential. In this case, half of two electrodes are

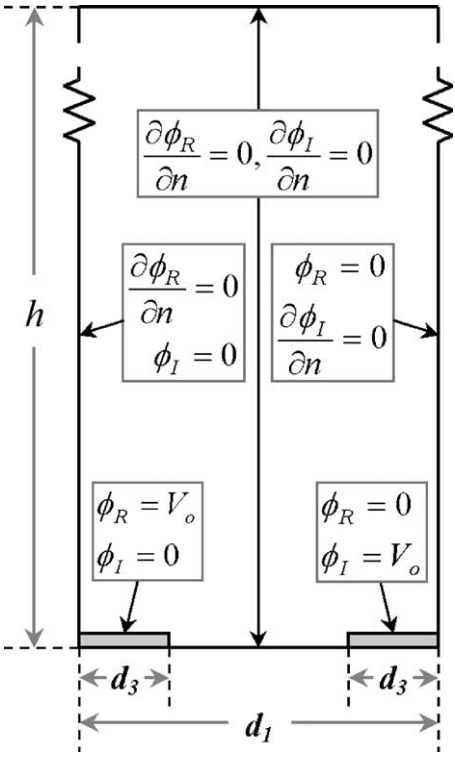


Fig. 6. The problem space for the travelling wave array showing the complete set of boundary conditions. The space covers half of each of two adjacent electrodes and the gap between. The width of the problem space was dimensional distance 2, equivalent to twice the dimensional parameter $d$. The height $h$ was much greater than the width of the problem space.

included in the problem space. The conditions for $\phi'_{\mathrm{R}}$ were: $\phi'_{\mathrm{R}} = 1$ on the left electrode and $\phi'_{\mathrm{R}} = 0$ on the right: on the left edge, the upper edge and the bottom edge between the electrodes, $\partial\phi'_{\mathrm{R}}/\partial n = 0$; and $\phi'_{\mathrm{R}} = 0$ on the right edge. The conditions for $\phi'_{\mathrm{I}}$ were: $\phi'_{\mathrm{I}} = 0$ on the left electrode and $\phi'_{\mathrm{I}} = 1$ on the right; on the right edge, the upper edge and the bottom edge between the electrodes, $\partial\phi'_{\mathrm{I}}/\partial n = 0$; and $\phi'_{\mathrm{I}} = 0$ on the left edge. The distance along the bottom edge is $2d$ which is a non-dimensional distance of 2, the height $h$ was defined to be 20. The electrode width was again $d_1$ and the gap width $d_2$ and the problem was initially solved with an electrode/width gap ratio of 1:1.

### 4.1. Results

The real and imaginary parts of the complex potential are shown in Fig. 7a and b. The vectors $\nabla'(|\nabla'\phi'_R|^2 + |\nabla'\phi'_I|^2) = \nabla'|\nabla'\tilde{\phi}'|^2$ and $\nabla' \times (\nabla'\phi'_{\mathrm{R}} \times \nabla'\phi'_{\mathrm{I}})$ for the DEP and twDEP components of the force (Eqs. (6) and (7)) were then calculated.

The vector $\nabla'|\nabla'\tilde{\phi}'|^2$ for the DEP force component is shown in Fig. 8a, again with the direction vectors plotted separately from the magnitude. Above $y' = 1$ ($y = d$), the vectors point straight towards the electrode plane and below, they tend more and more towards the electrode edges (at $x' = 0.5, 1.5$). As before, above $y' = 1$ the magnitude of $\nabla'|\nabla'\tilde{\phi}'|^2$ is constant with $x'$ across the array. Below this height, the magnitude increases to a maximum value at the electrode edges. The pattern of the vectors is symmetrical about a vertical line through the electrode edge, similar to the pattern of vectors for the DEP array.

The vector $\nabla' \times (\nabla'\phi'_{\mathrm{R}} \times \nabla'\phi'_{\mathrm{I}})$ for the twDEP component is shown in Fig. 8b. Above $y' \sim 1$, as for DEP component, the magnitude of this vector function is constant with $x'$ but the vectors this time point in the negative $x$-direction. It should be noted that in the force Eqs. (7) and (10) this component is preceded by a negative sign, so that for a positive value of Im[$\alpha$] the twDEP component points in the

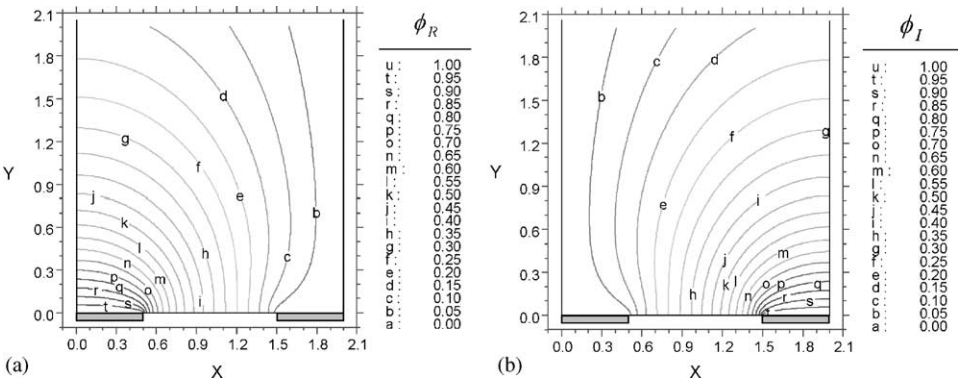


Fig. 7. The real (a) and imaginary (b) parts of the potential phasor, solved for the problem space of Fig. 6, shown for the $2 \times 2$ region close to the electrodes. Comparison of (a) and (b) shows that the solution for $\phi'_{\mathrm{I}}$ is the mirror image of that for $\phi'_{\mathrm{R}}$ about the line $x' = 1$ in the centre of the gap.

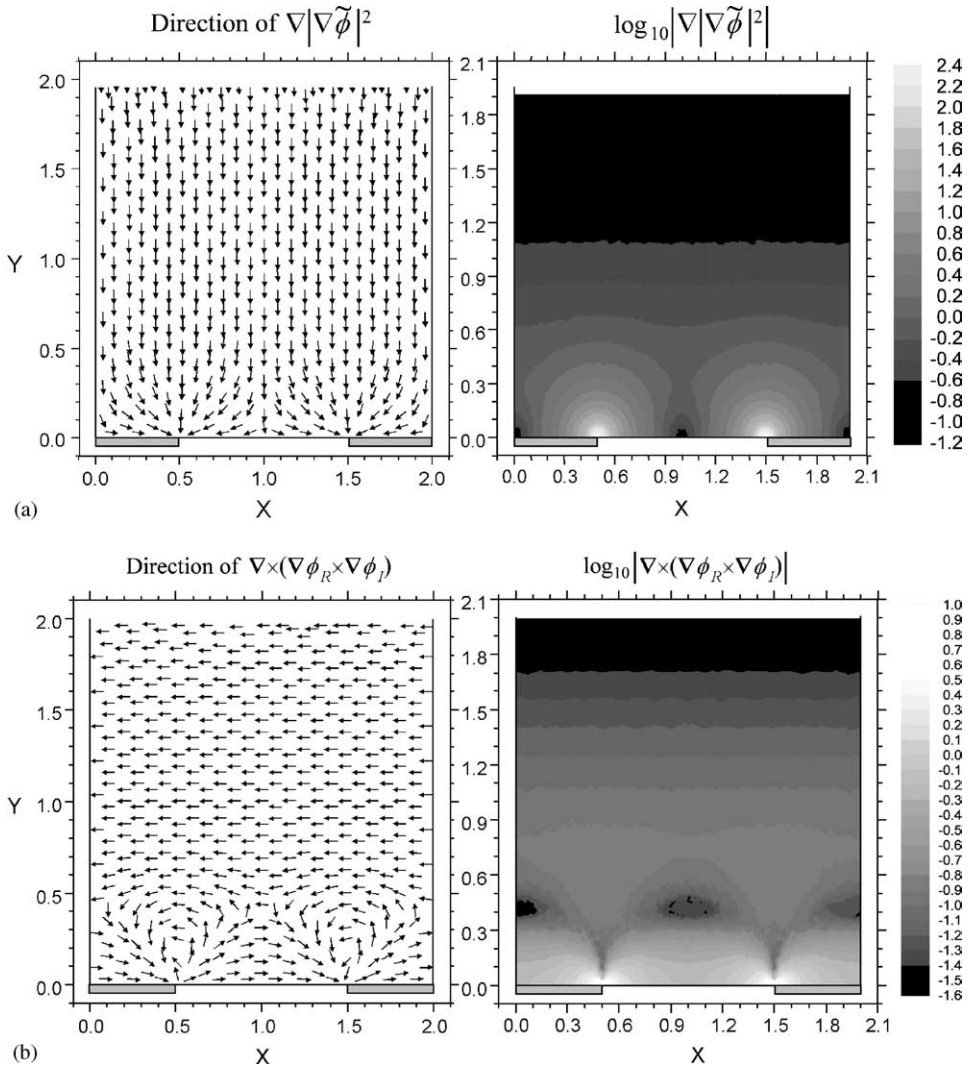


Fig. 8. (a) The vector for the DEP force component: $\nabla'|\nabla'\tilde{\phi}'|^2$ for the $2\times2$ region close to the electrodes plotted separately as vector direction and $\log_{10}$(magnitude). The maximum value of the magnitude is close to the electrode edges. (b) The vector for the twDEP force component: $\nabla'\times(\nabla'\phi'_R\times\nabla'\phi'_I)$ for the $2\times2$ region close to the electrodes. This is plotted separately as vector direction and $\log_{10}$(magnitude) and the maximum value of the magnitude is close to the electrode edges.

direction of increasing phase at distances far from the electrodes. Closer to the electrodes, the vectors exhibit a more complicated pattern, pointing in the opposite direction very close to the surface and moving in a circular pattern over the electrode edges. The magnitude of this vector function is also a maximum at the electrode edges.

Comparison of these numerical results with the pattern of vectors calculated from the Fourier series analysis [11] demonstrates that proper boundary conditions are essential if particle movement close to the electrodes is to be accurately modelled. Comparison of Fig. 8a in this work with Fig. 8 from Ref. [11] shows discrepancies in the pattern of the force vector direction close to the electrode edges. Further, comparison of the pattern for the vector $\nabla' \times (\nabla' \phi'_{\mathrm{R}} \times \nabla' \phi'_{\mathrm{I}})$, Fig. 8b in this work and Fig. 10 in Ref. [11] shows a substantial difference in the predicted motion of particles experiencing twDEP close to the electrodes.

In the region above $y' \sim 1$, the vector magnitudes were again matched to an exponential function Eq. (11), with the results shown in Fig. 9. Re-writing equations for the force components (10) and substituting for the normalised distance in the exponentials gives the total force for a spherical particle in the region $y > d$:

$$\langle \mathbf{F} \rangle = -A_{\mathrm{twDEP}} \upsilon \, \mathrm{Im}[\alpha] \frac{V_0^2}{d^3} \mathrm{e}^{(-k_{\mathrm{twDEP}} y/d)} \hat{x} - A_{\mathrm{DEP}} \upsilon \, \mathrm{Re}[\alpha] \frac{V_0^2}{d^3} \mathrm{e}^{(-k_{\mathrm{twDEP}} y/d)} \hat{\mathbf{y}}. \tag{13}$$

The values for the two coefficients, $A_{\mathrm{DEP}}$ and $A_{\mathrm{twDEP}}$, are given in Table 3 and agree with each other to within 0.05% and the two exponential factors were within 0.02% of $\pi/2$ as expected.

### 4.2. Comparison with Fourier series solution

Comparison of the coefficients with the values calculated from the Fourier series analysis in this case showed that the difference was 22.3%. This is an indication that the boundary condition on the lower surface is more critical for the twDEP array.

Again, to estimate the numerical error for this solution, the electrical potential was solved using the same linear boundary condition between the electrodes as was used

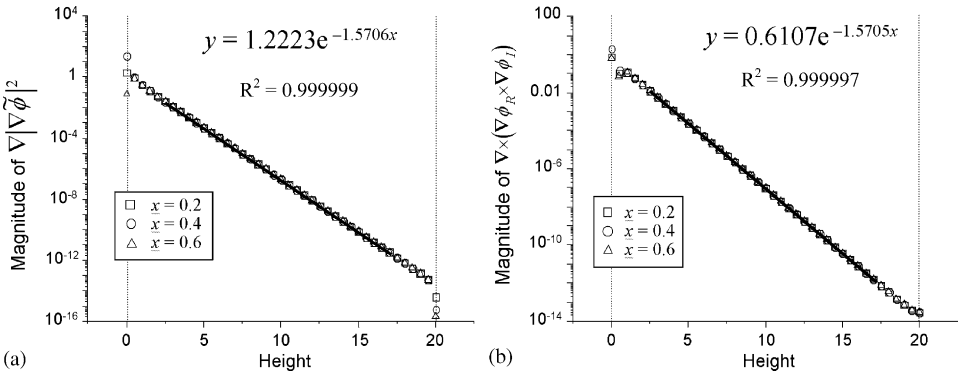


Fig. 9. The magnitude of (a) the vector $\nabla' |\nabla' \tilde{\phi}'|^2$ and (b) the vector $\nabla' \times (\nabla' \phi'_{\mathrm{R}} \times \nabla' \phi'_{\mathrm{I}})$ plotted along several vertical lines indicated by the legend. The two magnitudes follow exponentially decreasing functions above $y' \sim 1$ independent of $x$. The exponential matching functions are shown in the figures.

Table 3
Numerically calculated values of the coefficients for the exponential approximation of the DEP and twDEP components of the force for the travelling wave electrode array

| Boundary condition in gap | $k_{DEP}$ | $A_{DEP}$ | % difference from Fourier | $k_{twDEP}$ | $A_{twDEP}$ | % difference from Fourier |
|---|---|---|---|---|---|---|
| Numerical solution: Constant current $\partial\tilde{\phi}'/\partial n = 0$ | 1.5706 | 0.3050 | 22.3 | 1.5705 | 0.3049 | 22.3 |
| Numerical solution: linear potential | 1.5708 | 0.3732 | 0.074 | 1.5707 | 0.3728 | 0.033 |
| First-order Fourier expansion | $\pi/2$ | 0.37292 | | $\pi/2$ | 0.37292 | |

Table 4
Numerically calculated values of the coefficient $A_{DEP}$ and $A_{twDEP}$ in the exponential approximation of the dielectrophoretic force for a variety of electrode/gap ratios, as well as the values calculated from the Fourier series analysis and the percentage difference

| Electrode/gap ratio $d_1$:$d_2$ | $A_{DEP}/A_{twDEP}$ (Fourier) | $A_{DEP}$ (numerical) | Difference (%) | $A_{twDEP}$ (numerical) | Difference (%) |
|---|---|---|---|---|---|
| 4:1 | 0.38948 | 0.37938 | 2.7 | 0.37929 | 2.7 |
| 3:1 | 0.38768 | 0.37141 | 4.4 | 0.37132 | 4.4 |
| 2:1 | 0.38381 | 0.35415 | 8.4 | 0.35406 | 8.4 |
| 1:1 | 0.37292 | 0.30558 | 22.0 | 0.30535 | 22.1 |
| 1:2 | 0.35810 | 0.24195 | 48.0 | 0.24191 | 48.0 |
| 1:3 | 0.34933 | 0.20388 | 71.4 | 0.20385 | 71.3 |
| 1:4 | 0.34367 | 0.17928 | 91.7 | 0.17925 | 91.7 |

in the Fourier series analysis. The values for $k_{DEP}$ and $k_{twDEP}$ were the same as for the $\partial\tilde{\phi}'/\partial n = 0$ boundary condition and the values for $A_{DEP}$ and $A_{twDEP}$ matched the values calculated using the Fourier series analysis to 0.074% and 0.033%, respectively. The error can therefore be estimated to be of the order of 0.05%.

### 4.3. Different electrode/gap width ratios

The problem was solved for different ratios of electrode width $d_1$ to gap width $d_2$. The values for the exponential coefficients $k_{DEP}$ were, for all cases, within 0.05% of $\pi/2$ as expected. The values of $A_{DEP}$ and $A_{twDEP}$ for several different ratios are shown in Table 4, along with the value calculated from the Fourier series solution and the difference between the two expressed as a percentage.

As the ratio between the electrode and gap width increases, the numerically calculated value for $A_{DEP}$ increases and the difference between it and the Fourier series value decreases. Again, as the gap width decreases, the exact boundary

condition on the surface between the electrodes becomes less important in determining the force far from the electrodes.

### 4.4. Electrorotation

The vector for the electrorotational torque $\nabla'\phi'_{\mathrm{R}} \times \nabla'\phi'_{\mathrm{I}}$ was also calculated. Fig. 10 shows the magnitude of the electrorotational vector plotted in the $(2 \times 2)$ region close to the electrodes, again on a logarithmic scale. In these simulations, $\nabla'\phi'_{\mathrm{R}} \times \nabla'\phi'_{\mathrm{I}}$ always pointed in the same direction, in this case out of the page.

At heights above $y' \sim 1$, the magnitude of $\nabla'\phi'_{\mathrm{R}} \times \nabla'\phi'_{\mathrm{I}}$ and therefore the rate of rotation is constant with $x'$ for a given height. In this region, the magnitude of the torque can again be matched to an exponential function with $k_{\mathrm{ROT}}$ again equal to $\pi/2$ and the value of $A_{\mathrm{ROT}} = 0.3888$. The dimensional torque expression is, therefore

$$|\langle \Gamma \rangle| = A_{\mathrm{ROT}} \upsilon \, \mathrm{Im}[\alpha] \frac{V_0^2}{d^2} \mathrm{e}^{(-k_{\mathrm{ROT}} y/d)} \tag{14}$$

For this two-dimensional problem, the torque can be written as $\Gamma = \Psi\hat{\mathbf{z}}$. Since the twDEP force component is half of the curl of the torque, the contour lines of $\Psi$ are parallel to the twDEP component of the force (compare Figs. 8b and 10). In effect, since

$$\mathbf{F} = \tfrac{1}{2}\nabla \times (\Psi\hat{\mathbf{z}}) = \frac{1}{2}\left(\frac{\partial \Psi}{\partial y}\hat{\mathbf{x}} - \frac{\partial \Psi}{\partial x}\hat{\mathbf{y}}\right),$$

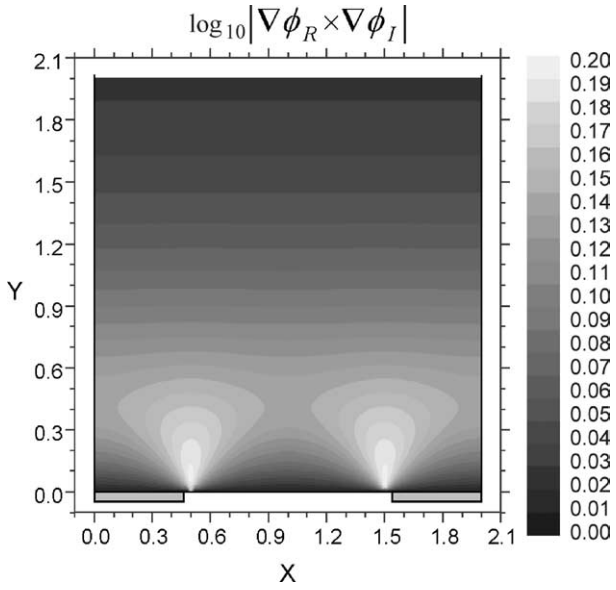


Fig. 10. The magnitude of the electrorotational torque $(\nabla'\phi'_{\mathrm{R}}) \times (\nabla'\phi'_{\mathrm{I}})$ plotted as contours on a $\log_{10}$ scale for the $2 \times 2$ region close to the electrodes and for ratios of electrode width to gap width of 1:1.

where **F** is perpendicular to the gradient of $\Psi$ and, therefore, parallel to the isolines of $\Psi$. This is true only if the problem is two dimensional.

Experimentally, if the rotational motion of the particle in the $x-y$ plane were observed, this would provide an additional independent measurement of Im[$\alpha$], which is one objective of the experiments. This would then allow field driven particle motion and fluid flow to be distinguished.

## 5. Conclusion

A methodology for exploring the numerical simulation of the DEP force in complex electric fields has been described and implemented. This method provides a fast and simple way of determining DEP and travelling wave forces, as well as the electrorotational torque for electrode arrays.

The DEP force for parallel, coplanar, bar electrodes used in DEP and twDEP experiments has been numerically calculated using the finite element method. The calculated values of the forces have been compared with previous analytical results.

The inaccuracies in far field solutions resulting from the use of different boundary conditions in analytical approximations such as the Fourier series analysis have been highlighted. The boundary conditions used in the numerical work are more physically reasonable, being derived from the condition of charge conservation.

## Acknowledgements

N.G. Green is a Royal Academy of Engineering Post Doctoral Research Fellow at the University of Glasgow. The authors would also like to acknowledge the support of the European Union for awarding a Marie Curie fellowship (contract no. BIO4-CT98-5010 (DG12-SSMI)) to N.G. Green and the Spanish Government Agency Dirección General de Ciencia y Tecnologia under contract BFM2000-1056.

## References

[1] T.B. Jones, Electromechanics of Particles, Cambridge University Press, Cambridge, 1995.
[2] R. Pethig, Dielectrophoresis: using inhomogeneous AC electrical fields to separate and manipulate cells, Crit. Rev. Biotechnol. 60 (1996) 331–348.
[3] G.H. Markx, Y. Huang, X.-F. Zhou, R. Pethig, Dielectrophoretic characterization and separation of microorganisms, Microbiology, UK 140 (1994) 585–591.
[4] H. Morgan, M.P. Hughes, N.G. Green, Separation of submicron bioparticles by dielectrophoresis, Biophys. J. 77 (1999) 516–525.
[5] G.H. Markx, R. Pethig, J. Rousselet, The dielectrophoretic levitation of latex beads, with reference to field-flow fractionation, J. Phys. D: Appl. Phys. 30 (1997) 2470–2477.
[6] Y. Huang, X.-B. Wang, F.F. Becker, P.R.C. Gascoyne, Introducing dielectrophoresis as a new force field for field-flow fractionation, Biophys. J. 73 (1997) 1118–1129.
[7] R. Hagedorn, G. Fuhr, T. Muller, J. Gimsa, Traveling-wave dielectrophoresis of microparticles, Electrophoresis 13 (1992) 49–54.

[8] M.S. Talary, J.P.H. Burt, J.A. Tame, R. Pethig, Electromanipulation and separation of cells using travelling electric fields, J. Phys. D: Appl. Phys. 29 (1996) 2198–2203.
[9] X.-J. Wang, X.-B. Wang, F.F. Becker, P.R.C. Gascoyne, A theoretical method of electrical field analysis for dielectrophoretic electrode arrays using Green's theorem, J. Phys. D: Appl. Phys. 29 (1996) 1649–1660.
[10] S. Masuda, M. Washizu, M. Iwadare, Separation of small particles suspended in liquid by nonuniform traveling field, IEEE Trans. Ind. Appl. IA-23 (1987) 474–480.
[11] H. Morgan, A.G. Izquierdo, D. Bakewell, N.G. Green, A. Ramos, The dielectrophoretic and travelling wave forces generated by interdigitated electrode arrays: analytical solution using Fourier series, J. Phys. D: Appl. Phys. 34 (2001) 1553–1561, Erratum: J. Phys. D: Appl. Phys. 34 (2001) 2708.
[12] T. Schnelle, R. Hagedorn, G. Fuhr, S. Fiedler, T. Muller, 3-Dimensional electric-field traps for manipulation of cells—calculation and experimental-verification, Biochim. Biophys. Acta 1157 (1993) 127–140.
[13] X.-B. Wang, Y. Huang, J.P.H. Burt, G.H. Markx, R. Pethig, Selective dielectrophoretic confinement of bioparticles in potential—energy wells, J. Phys. D: Appl. Phys. 26 (1993) 1278–1285.
[14] M.P. Hughes, R. Pethig, X.-B. Wang, Dielectrophoretic forces on particles in travelling electric fields, J. Phys. D: Appl. Phys. 28 (1995) 474–482.
[15] O.C. Zienkiewicz, The Finite Element Method, McGraw-Hill, London, 1977.
[16] P. Lorrain, D.R. Corson, F. Lorrain, Fundamentals of Electromagnetic Phenomena, Freeman, New York, 2000.
[17] H.A. Haus, J.R. Melcher, Electromagnetic Fields and Energy, Prentice-Hall, Englewood Cliffs, NJ, 1989.
[18] www.pdesolutions.com.
[19] N.G. Green, A. Ramos, H. Morgan, AC electrokinetics: a survey of sub-micrometre particle dynamics, J. Phys. D: Appl. Phys. 33 (2000) 632–641.
[20] X.-B. Wang, Y. Huang, F.F. Becker, P.R.C. Gascoyne, A unified theory of dielectrophoresis and traveling-wave dielectrophoresis, J. Phys. D: Appl. Phys. 27 (1994) 1571–1574.